SAKARYA ÜNİVERSİTESİ
FEN BİLİMLERİ ENSTİTÜSÜ DERGİSİ

Sakarya University Journal of Science
SAUJS

ISSN 1301-4048 e-ISSN 2147-835X Period Bimonthly Founded 1997 Publisher Sakarya University
http://www.saujs.sakarya.edu.tr/

Title: Synthesis and Structural Investigations of 1, 2-bis(2-ethoxybenzylidene)hydrazine

Authors: Sevgi KANSIZ

Recieved: 2022-02-02 00:00:00

Accepted: 2023-03-02 00:00:00

Article Type: Research Article

Volume: 27
Issue: 4
Month: August
Year: 2023
Pages: 768-780

How to cite
Sevgi KANSIZ; (2023), Synthesis and Structural Investigations of 1, 2-bis(2-ethoxybenzylidene)hydrazine. Sakarya University Journal of Science, 27(4), 768-780, DOI: 10.16984/saufenbilder.1227659
Access link
https://dergipark.org.tr/en/pub/saufenbilder/issue/79486/1227659

Sakarya University Journal of Science 27(4), 768-780, 2023

Synthesis and Structural Investigations of 1, 2-bis(2-ethoxybenzylidene)hydrazine

Sevgi KANSIZ *1

Abstract

The titled compound, 1,2-bis(2-ethoxybenzylidene) hydrazine was developed using the reaction of 2-ethoxybenzaldehyde and hydrazine monohydrate in an ethanolic solution. In the Schiff-based hydrazine compound, $C_{18}H_{20}N_2O_2$, the mid-point of the nitrogen atoms of the central hydrazine moiety is located in inversion symmetry. In $C_{18}H_{20}N_2O_2$, C−H···N hydrogen bond linked the molecules, and the framework stabilized by weak C−H···π and π···π stacking interactions. MEP, HOMO and LUMO analysis were performed with the DFT/B3LYP method and the 6-311+G(d,p) basis set. The energies of frontier orbitals were calculated to understand specific molecular properties such as electronegativity, chemical reactivity, chemical hardness and softness. For investigating the contributions of various intermolecular contacts within the hydrazine compound, Hirshfeld surface analysis was performed. The largest contribution of the compound to the main interactions comes from the H···H (64%), C···H (16%) and N···H (9%) interactions.

Keywords: Schiff base, hydrazine, X-ray, DFT, Hirshfeld surface analysis

1. INTRODUCTION

Schiff base compounds are among the important inorganic materials due to their flexibility in coordination geometries, forming many metal complexes, easy synthesis and stability of their compounds [1-5]. Schiff base compounds are small molecules that are obtained as a result of the nucleophilic addition reaction of aldehydes or ketones with primary amines and contain carbon-nitrogen double bonds (-CH=N) [6]. Schiff base ligands can form highly stable 4, 5, or 6-ring aromatic compounds. For this, it is necessary having a second functional group close to the azomethine group and a displaceable hydrogen atom. This group is preferably the hydroxyl group. Schiff base compounds, which are used extensively in the field of coordination chemistry due to their electron-donating ability, are used in many new areas [7] from the health field [8] to the dyeing industry [9] due to their properties such as electroluminescence effects [10], fluorescence [11], and nonlinear optics [12]. Hydrazine, which is a strong reducing agent, is frequently used in areas such as various industrial, pharmacological, and many other applications [13, 14]. Hydrazine derivatives having a wide range of uses as an intermediate in the synthesis of pharmaceutical drugs, as a polymerization catalyst and in plastic

* Corresponding author: sevgi.kansiz@samsun.edu.tr (S. KANSIZ)
[1] Samsun University, Faculty of Engineering, Department of Fundamental Sciences, Samsun, Türkiye
ORCID: https://orcid.org/0000-0002-8433-7975

processing, are also considerably used as a technological compound in the magnetic and biomedical fields [15].

In this study, a hydrazine-Schiff base compound, $C_{18}H_{20}N_2O_2$, 1,2-bis(2-ethoxybenzylidene) hydrazine was synthesized as a result of the condensation reaction of 2-ethoxybenzaldehyde and hydrazine monohydrate in an ethanolic solution. The theoretical calculations of the Schiff-based hydrazine compound, its structure was identified by the X-ray diffraction technique, were compared with the data obtained from the crystallographic analysis. In order to examine the theoretical structure of the 1,2-bis(2-ethoxybenzylidene) hydrazine molecule, the Gaussian package program was used and its three-dimensional approximate geometry was drawn in the GaussView program [16, 17]. In all theoretical calculations, the density functional method (DFT) and Becke type 3-parameter Lee-Yang-Par model (B3LYP) and 6-311+G(d,p) basis set were used [18]. After optimization, the frontier molecular orbitals energies, global hardness and softness parameters, electrophilic and nucleophilic regions on the molecular electrostatic potential map were determined, and the results were evaluated under these headings. In addition, visual representation of d_{norm}, shape index, and curvedness maps obtained by Hirshfeld surface analysis, percent contribution of atoms to interactions, and two-dimensional fingerprint determinations were obtained using the Crystal Explorer program [19].

1.1. Crystallographic Part

An appropriate single crystal was selected for the Schiff-based hydrazine derivative compound and data collection was obtained by STOE IPDS 2 image plate detector using MoKα radiation (λ = 0.71073Å). X-AREA as used for data collection and cell enhancement and X-RED was used for data reduction [20]. The structure of the Schiff-based hydrazine derivative compound was determined using the SHELXT structure solution program [21]. The direct methods were employed to solve the structure of the compound, followed by refinement using full-matrix least-squares techniques on F^2 using SHELXL [22]. The refinement was carried out against all reflections to ensure a thorough and accurate analysis of the structure. In the refinement process, the hydrogen atoms were constrained by difference maps, which allowed for a more precise determination of their positions. The hydrogen atoms were also refined isotropically, meaning that their thermal motion was assumed to be the same in all directions. In contrast, all non-hydrogen atoms were refined anisotropically, which means that their thermal motion was allowed to vary depending on the direction. This approach ensured that the most accurate positions and thermal parameters were determined for each atom in the compound. Detailed parameters of the crystal structure are given in Table 1.

Table 1 Experimental details of the title compound

CCDC number	2177378
Chemical formula	$C_{18}H_{20}N_2O_2$
Mr	296.36
Radiation type	Mo K\a
Wavelength	0.71073
Crystal System, Space Group	Monoclinic, $P2_1/c$
Data collection Diffractometer	STOE IPDS 2
Temperature	296
a, b, c (Å)	7.6871(11), 11.7638(11), 9.0832(12)
α, β, γ	90, 102.257(10), 90
Cell Volume, V	802.67(18)
μ (mm^{-1})	0.08
Absorption correction	integration
No. of measured, independent and observed [I > 2σ(I)] reflections	7323, 2592, 1505
No. of reflections	2592
No. of parameters	101
Crystal Size	0.75 x 0.67 x 0.58
F(000)	316
Theta range for data collection	1.7−31.6
Z	2
Limiting Indices	$-9 \le h \le 11$, $-14 \le k \le 17$, $-13 \le l \le 13$
R_{int}	0.052
Final R Indices [$F^2 > 2\sigma(F^2)$], wR(F^2), S	0.046, 0.128, 0.99
$\Delta\rho_{max}$, $\Delta\rho_{min}$ ($e/Å^3$)	0.18, −0.14

1.2. Methods

The utilization of DFT calculations with various parameters and analyses provides a comprehensive understanding of a molecule's electronic properties, reactivity, and stability. This knowledge can guide the design and synthesis of new compounds with desired properties. In this study, DFT was employed to optimize the molecular structure of the compound utilizing the B3LYP functional and the 6-311+G(d,p) basis set. The B3LYP functional is a hybrid functional that combines the Becke three-parameter exchange functional and the Lee-Yang-Parr correlation functional. The optimized structure was evaluated for stability using frontier orbitals (HOMO and LUMO) and susceptibility to chemical activity was also explored. Chemical activity parameters such as kinetic stability, chemical stability, and intramolecular charge transfer were also determined. Additionally, molecular electrostatic potential (MEP) analysis was used to identify electron-rich and poor regions. The optimized geometry of the compound, MEP map, and HOMO-LUMO energy gaps were visualized using the GuassView 5.0 software.

The analysis of Hirshfeld surfaces [23, 24], along with their corresponding two-dimensional (2D) fingerprint plots, is a powerful tool for investigating intermolecular interactions within a crystal structure [25-27]. The Hirshfeld surface is generated by mapping the electron density of a crystal structure onto a three-dimensional grid surrounding the molecule. Subsequent analysis of the surface provides information about intermolecular interactions within the crystal, such as the location and strength of hydrogen bonds and other non-covalent interactions. The d_{norm} property, which is used in this analysis, is a measure of the normalized contact distance between two atoms within a crystal structure. This property is defined in terms of the van der Waals (vdW) radii of the atoms, as well as the distances between their respective vdW surfaces. A 2D fingerprint plot is used to visualize the combination of the de and di properties of the Hirshfeld surface. This tool can be used to identify specific regions of the surface that correspond to particular types of intermolecular interactions and to compare the surface properties of different crystal structures. To perform these calculations and generate visualizations of the Hirshfeld surfaces and their associated 2D fingerprint plots, the Crystal Explorer 21 software package was employed.

1.3. Synthesis of 1,2-bis(2-ethoxybenzylidene) hydrazine

To synthesize 1,2-bis(2-ethoxybenzylidene) hydrazine, a solution of 2-ethoxybenzaldehyde (1.50 g, 10 mmol) in 10 mL of ethanol was added to a solution of hydrazine monohydrate (65%) (0.38 g, 5 mmol) in 5 mL of ethanol with constant stirring at 0°C. The resulting mixture was stirred at room temperature for 12 hours until a light-yellow solid precipitated. The mixture was then filtered and washed with cold ethanol before being left to dry at room temperature. The obtained solid was recrystallized from ethanol, resulting in a yield of 82% (1.45 g, 4.9 mmol) (Figure 1).

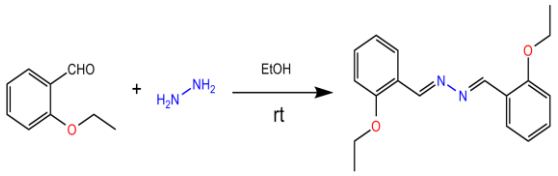

Figure 1 Synthesis of the title compound

2. CONCLUSIONS AND DISCUSSION

2.1. Crystal Structure of $C_{18}H_{20}N_2O_2$

The structure of the Schiff base hydrazine derivative mentioned in the title is presented in Figure 2. It is important to note that the asymmetric unit of this compound comprises one-half of the centrosymmetric molecule. X-ray analysis revealed that the Schiff-based hydrazine derivate compound, $C_{18}H_{20}N_2O_2$, crystallizes in the $P2_1/c$ space group in the monoclinic system. Unit cell parameters; a = 7.6871(11), b = 11.7638(11), c = 9.0832(12)

Å, α=90°, β= 102.257(10)° and γ= 90°. The conformation of the Schiff base is nearly coplanar, which is evident from the C2—C1—N1—N1^{i} torsion angle of 179.65 (12)°. This observation is further supported by the C3—C2—C1—N1 torsion angle of 6.29 (18)°, which confirms that the phenol ring and the Schiff base are coplanar. The bond lengths of C7–O1 and C8–O1 are 1.3612(14) Å and 1.4284(13) Å, respectively (Table 2). These values are in agreement with the standard values reported for single C—O bonds [28-30]. The bond lengths of C7–O1 and C8–O1 were calculated as 1.3613 Å and 1.4283 Å, respectively. These values are in close agreement with the experimental data obtained from the X-ray crystal structure, as illustrated in Figure 1, indicating that the DFT calculations accurately predicted the molecular geometry of the compound. The C1—N1 bond is notably short, measuring 1.2659 (13) Å, indicating the presence of a C=N double bond. In contrast, the hydrazine bond length of N1—N1^{i} is relatively long, measuring 1.4059(17) Å, which suggests that a single bond exists. The N—N hydrazine bond length observed in this study appears to be consistent with previously reported values. While the value obtained in this study is 1.4059 (17) Å, which is slightly longer than the reported range of 1.360-1.376 Å [31-33] in other studies, this difference is not significant enough to suggest any discrepancies between the current results and previously reported values. Overall, these findings support the reliability and validity of the experimental measurements and provide useful information for further investigations of the electronic and chemical properties of the compound. Likewise, C7-O1-C8, C1-N1-N1^{i} and C2-C1-N1 bond angles were obtained as 117.93(8)º, 112.75(12)º and 121.97(11)º. The bond angles of C7-O1-C8, C1-N1-N1^{i} and C2-C1-N1 were calculated as 117.9372º, 112.7641º and 121.9653º, respectively. The good agreement between the calculated and experimental bond lengths and angles underscores the reliability and utility of DFT as a tool for predicting and understanding the properties and reactivity of molecules. In this way, the calculated bond lengths and angles provide valuable insights into the electronic structure and bonding patterns of the molecule, which are critical for understanding its chemical behavior. Therefore, the consistency between the optimized geometry given by the DFT calculations and the experimental crystal structure is a positive indication of the quality of the calculations and the confidence that can be placed in the results.

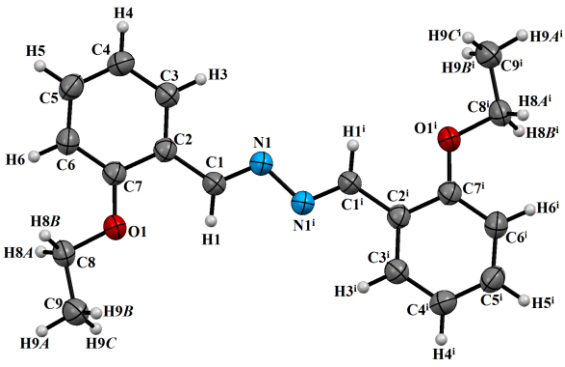

X-Ray

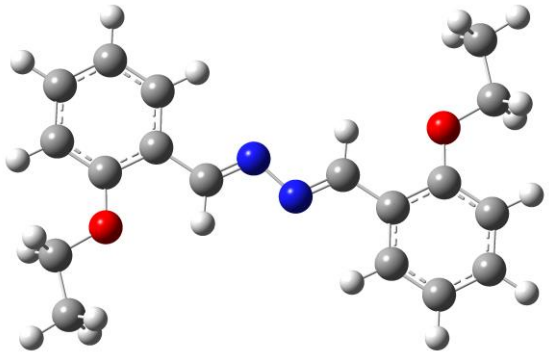

DFT

Figure 2 Molecular structure of the title compound

The molecules in $C_{18}H_{20}N_2O_2$ are linked by C4−H4···N1^{i} hydrogen bond (Table 3). C4 atom (symmetry code: x, y, z) acts as a donor and forms C−H···N hydrogen bonds with the N1 atom (symmetry code: *x*, −*y*−1/2, *z*−1/2). In this interaction, the distances between the atoms of C4−H4 (D−H), H4···N1 (H···A) and C4···N1 (D···A) were obtained as 0.93, 2.62(3) and 3.5476(12) Å, respectively. Additionally, C8−H8*B*···Cg1 and π···π stacking interactions between the benzene rings stabilized the molecular structure, inhere *Cg*1 is the centered of the benzene ring and *Cg*1···*Cg*1 distance is 3.6442(12) Å with

a slippage of 0.659 Å. Some interactions are shown in Figure 3.

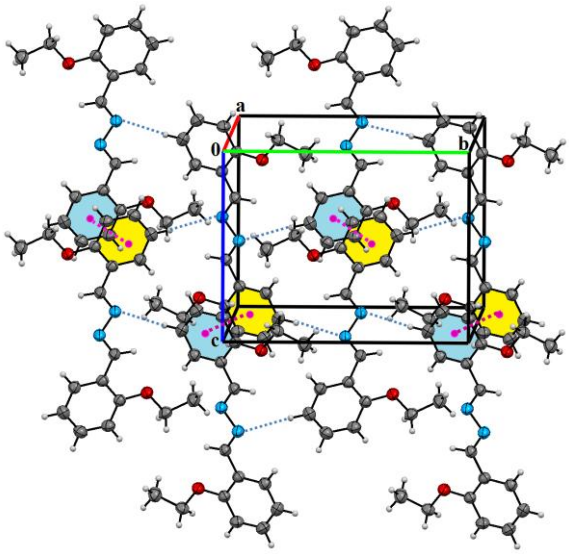

Figure 3 The crystal packing of the title compound

Table 2 Some selected geometric parameters for the title compound

Bond	(Å)	Angle	(deg)
N1−N1^{i}	1.4059(17)	C7−O1−C8	117.93(8)
C7−O1	1.3612(14)	C9−C8−O1	107.43(9)
C8−O1	1.4284(13)	C2−C7−O1	116.05(9)
C1−N1	1.2659(13)	C6−C7−O1	124.32(10)
C1−C2	1.4578(14)	C2−C1−N1	121.97(11)
C8−C9	1.4959(18)	C1−N1−N1^{i}	112.75(12)
C2−C3	1.3897(16)	C3−C2−C1	121.33(9)
C3−C4	1.3747(15)	C7−C2−C1	119.98(10)
C7−C2	1.4046(15)	C4−C3−C2	121.31(10)

Table 3 Interactions geometries in the title compound

D−H···A	D−H	H···A	D···A	D−H···A
C4−H4···N1^{i}	0.93	2.62	3.5476(12)	178(2)
C8−H8*B*···Cg1^{ii}	0.97	2.84	3.6689(12)	144(2)

Symmetry codes: (i) *x*, −*y*−1/2, *z*−1/2; (ii) −*x*, −*y*, −*z*.

2.2. Molecular Orbitals of $C_{18}H_{20}N_2O_2$

The ability of a molecule to donate electrons is defined as the HOMO energy (E_{HOMO}), while the ability to accept electrons is defined as the LUMO energy (E_{LUMO}). The electronic properties and reactivity of the Schiff-based hydrazine derivative compound were investigated by performing DFT calculations in the gas phase environment. To gain further insight into the electronic structure of the molecule, the HOMO and LUMO surface views are given in Figure 4. Upon conducting this study, it was found that the energy gap for the compound was obtained as $\Delta E = 3.77$ eV, and it was predicted that the optimized structure under investigation is stable. The parameters of hardness and softness for a molecule optimized in a gas phase environment are calculated based on the HOMO and LUMO orbital energies. The chemical hardness and softness parameters are important descriptors of the electronic properties and reactivity of a molecule [34-37]. The hardness parameter is defined as the resistance of a molecule to electron transfer and is calculated as the average of the energy difference between the HOMO and LUMO orbitals. A high hardness value indicates that the molecule has a strong resistance to electron transfer and is less reactive. On the other hand, the softness parameter is defined as the inverse of the hardness and represents the ease with which the molecule can undergo electron transfer. A low softness value indicates that the molecule is more reactive and has a higher tendency to undergo chemical reactions. These parameters can be used to predict the stability and reactivity of a molecule under different conditions and can provide valuable insights into the chemical properties of the compound. In this study, the hardness and softness parameters of the Schiff-based hydrazine derivative compound were calculated as 1.89 $(eV)^{-1}$ and 0.26 eV, respectively, indicating a high chemical hardness and low softness (Table 4). This high hardness value, combined with its low softness value, suggests that the molecule has high kinetic stability and low chemical activity, indicating its potential for use as a stable compound in various applications.

To further assess the stability of the molecule, chemical activity parameters, such as chemical potential, electronegativity, and hardness, were calculated. Chemical potential represents the energy required to add an electron to a system, and electronegativity indicates the tendency of an atom to attract

electrons. A high hardness value indicates a greater resistance of the molecule to electron transfer, whereas a low softness value indicates a greater tendency of the molecule to undergo chemical reactions. The studied molecule was found to have high chemical hardness, suggesting very little intramolecular charge transfer and a greater resistance to electron transfer. This suggests that the molecule has high kinetic stability and low chemical reactivity, making it a promising candidate for further studies in the field of organic synthesis and medicinal chemistry.

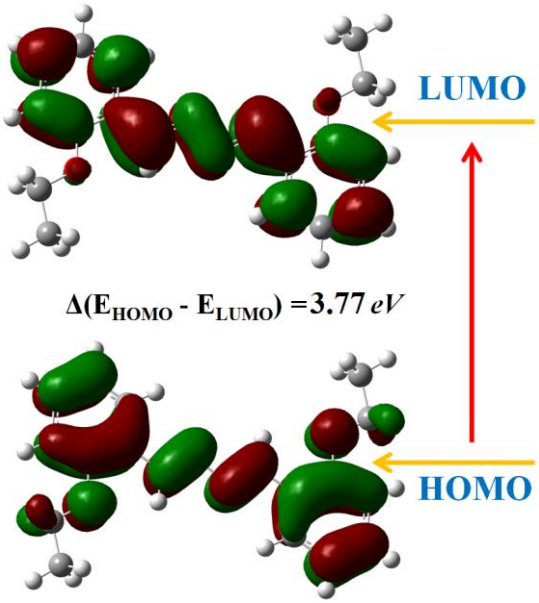

Figure 4 The frontier molecular orbitals of the title compound

Table 4 The HOMO-LUMO and related descriptors of the title compound

Parameters	$C_{18}H_{20}N_2O_2$
E_{LUMO} (eV)	-1.98
E_{HOMO} (eV)	-5.75
Energy band gap $\lvert E_{HOMO} - E_{LUMO} \rvert$	3.77
Ionization potential ($I = -E_{HOMO}$)	5.75
Electron affinity ($A = -E_{LUMO}$)	1.98
Chemical hardness ($\eta = (I-A)/2$)	1.89
Chemical softness ($\zeta = 1/2\eta$)	0.26
Electronegativity ($\chi = (I+A)/2$)	3.86
Chemical potential ($\mu = -(I+A)/2$)	-3.86

2.3. Molecular Electrostatic Potential

Molecular electrostatic potential (MEP) is a valuable tool in understanding the reactivity and behavior of molecules [38-42]. It is a graphical representation of the electrostatic potential energy of a molecule at different points on its surface. MEP is calculated using quantum mechanical calculations, and the resulting MEP surface is often displayed using a color scale to highlight regions of positive or negative potential. In general, regions of high positive potential on an MEP surface correspond to electrophilic regions, while regions of high negative potential correspond to nucleophilic regions. The color scale you mentioned is often used to interpret the MEP surface, with red indicating the most positive potential and blue indicating the most negative potential. Intermediate colors such as orange, yellow, green are used to indicate potential values between these extremes. MEP can be used to predict how a molecule might react with other molecules or reagents, as electrophilic molecules will tend to react with nucleophilic molecules. Additionally, MEP can provide insights into the behavior of biological molecules, such as enzymes and receptors, by highlighting regions of the molecule that are most likely to interact with other molecules.

The MEP surface is given in Figure 5. The electron-poor region in the neutral molecule is coded in blue, while the electron-rich regions appear in red. The red spots positioned on nitrogen atoms are the most negative regions. These regions represent regions that are active in the formation of hydrogen bonds and have a high electrophilic affinity. Regions with the most positive nucleophilic nature are located in regions where hydrogen atoms are concentrated. The electronegativity of benzene rings showed a redshift. On the MEP top surface, there is a representation of the electron density in the form of two-dimensional surface curves. The fact that the structure is prone to chemical activity and the presence of intramolecular and intermolecular hydrogen bonds predict that the electrophilic nature of the structures is more dominant.

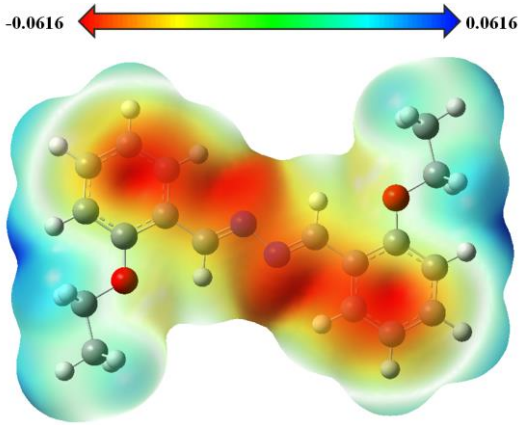

Figure 5 MEP map of the title compound

2.4. Hirshfeld Surface Analysis

The Hirshfeld surface analysis was employed as a tool to visualize the Van der Waals distances and identify intermolecular interaction points. Two-dimensional fingerprint determination was also carried out using Hirshfeld surface analysis to determine the percentage of interactions of atoms within the molecule. The equation for d_{norm} used in Hirshfeld surface analysis is defined as:

$$d_{norm} = (d_i - ri^{vdw})/ri^{vdw} + (d_e - re^{vdw})/re^{vdw}$$

Here, ri^{vdw} represents the Van der Waals radius of the atom inside the surface, while re^{vdw} represents the Van der Waals radius of the atom outside the surface. The values of d_i and d_e represent the separations between the closest atoms inside and outside the surface, respectively. The d_{norm} value ranges between -1 and 1, where negative values represent contact regions shorter than the sum of the Van der Waals radii, while positive values represent regions with longer separations. The d_{norm} values close to zero indicate the absence of any interatomic interaction. Thus, the d_{norm} function is used to visualize the intermolecular contacts and non-covalent interactions between atoms in a molecule, providing information about the geometry and strength of these interactions. The Hirshfeld surface maps of d_{norm}, shape index, and curvedness (Figure 6) are used to analyze the intermolecular interactions and molecular packing in a crystal structure [43-47]. The shape index is a measure of the local curvature of the surface and can be used to identify regions of the surface where there are π···π interactions between molecules. The curvedness, on the other hand, is a measure of the global curvature of the surface and can be used to identify regions where there are hydrogen bonds or other types of intermolecular interactions.

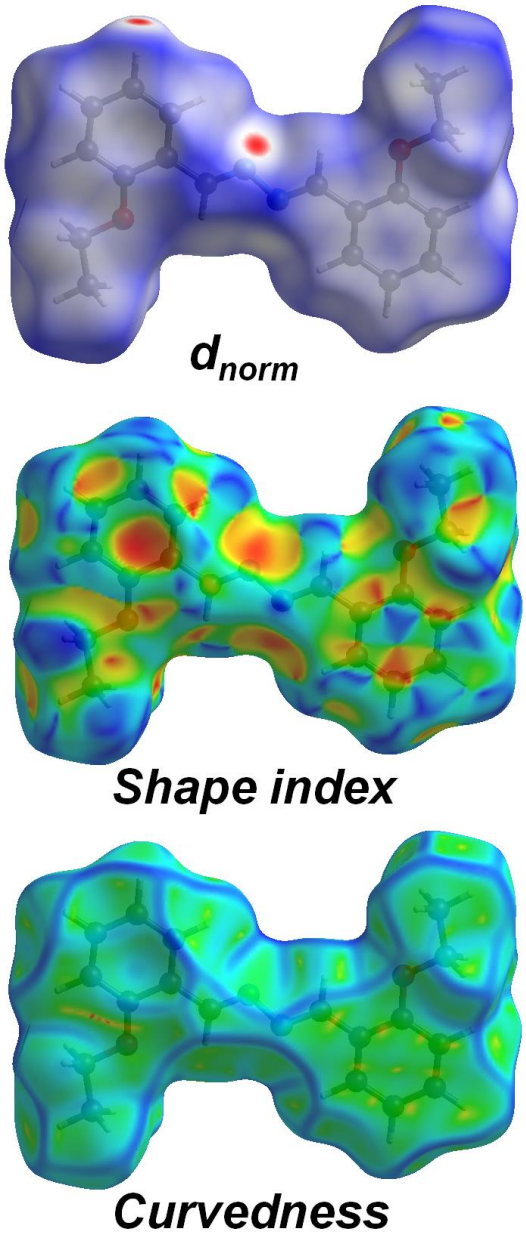

Figure 6 Hirshfeld surfaces of the title compound

Figure 6 presents the Hirshfeld surface maps that show the d_{norm}, shape index, and curvedness maps. The d_{norm} function is the most basic surface map that visualizes the contact areas shorter than the sum of the Van der Waals radius, and these regions are

colored in red. The blue-colored regions, on the other hand, represent intermolecular distances that are longer than the sum of the Van der Waals radii. The indices of the d_{norm} surface ranged between -0.1269 and 1.2504, while the shape index and curvedness were obtained between -1 and 1 and -4 and 4, respectively. The shape index provides a description of planar π···π interactions between molecules, which are represented by adjacent red and blue triangles in the shape index of the Hirshfeld surface.

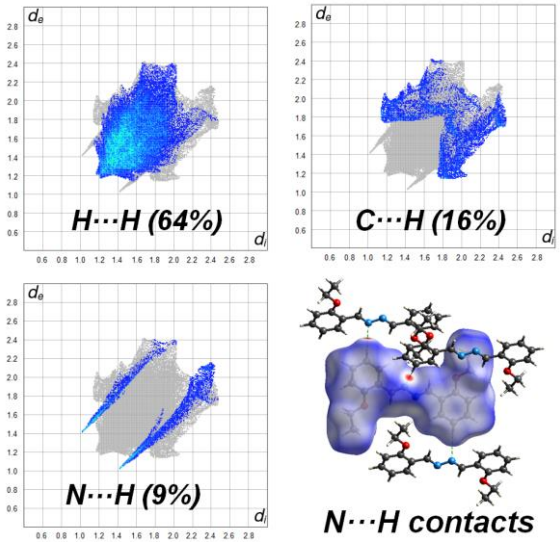

Figure 7 Two-dimensional fingerprint plots for the title compound

Additionally, hydrogen bonds on the Hirshfeld d_{norm} surface were shown in Figure 6, where the regions colored in red clearly demonstrated the presence of hydrogen bonds. Figure 7 shows the two-dimensional fingerprint maps, which indicate the contributions of different types of intermolecular interactions to the total Hirshfeld surface. H···H interactions accounted for the largest contribution to the total Hirshfeld surface (64%), followed by C···H (16%), N···H (9%), C···C (6.6%), O···H (3.7%), and C···O (1.7%), as shown in Figure 8. Overall, the Hirshfeld surface analysis provided valuable insights into the intermolecular interactions and the molecular properties of the compound.

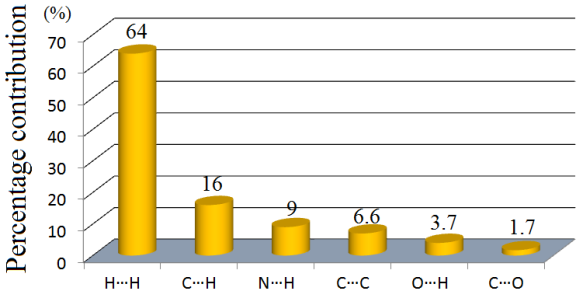

Figure 8 Intermolecular interactions with percentages in the title compound

3. CONCLUSION

In this study, the chemical activity and other calculations of the 1,2-bis(2-ethoxybenzylidene) hydrazine molecule, that structure was elucidated by X-ray diffraction analysis, was performed using Density Functional Theory (DFT). Theoretical computational methods allow us to have information about properties that cannot be obtained experimentally and to determine the chemical active site in advance. In this way, it helps us to make predictions about the molecular groups to be synthesized. In this context, the geometric parameters obtained from X-ray diffraction were compared with the geometric parameters obtained from the DFT method. Consequently, it revealed that the results are close to the experimental data. The hardness (1.89 eV) and softness (0.26 $(eV)^{-1}$) values of the optimized structure, whose energy range was calculated as 3.77 eV, predict that the molecule is quite stable with low chemical activity. In the MEP map, the most negative regions were illustrated in red on the nitrogen atoms, and these regions represent regions that are active in the formation of hydrogen bonds and have a high electrophilic affinity. The regions with the dominant nucleophilic nature are located in the regions where hydrogen atoms are concentrated. With Hirshfeld surface maps, the package structure and molecular interactions of the molecular structure were obtained and visualized. As a result of the Hirshfeld surface analysis, it was noticed that the H····H (64%) and C···H (16%) interactions made the greatest contribution to the Hirshfeld surface.

In summary, the Schiff-based hydrazine derivative compound was subjected to a comprehensive characterization using several analytical techniques, including single-crystal X-ray diffraction, DFT studies, and Hirshfeld surface analysis. The crystallographic data obtained from the X-ray diffraction experiment was in good agreement with the results of the DFT calculations and Hirshfeld surface analysis. The DFT studies provided a detailed understanding of the electronic properties, stability, and reactivity of the compound, while the Hirshfeld surface analysis allowed for the identification of specific intermolecular interactions in the crystal structure. Overall, the combined use of these techniques provided a thorough characterization of the compound and a deeper understanding of its properties and behavior.

Acknowledgments
The author would like to thank Assoc. Prof. Dr. Mustafa Kemal Gümüş and Assoc. Prof. Dr. Necmi Dege for their contributions.

Funding
The author (s) has no received any financial support for the research, authorship or publication of this study.

Authors' Contribution
The authors contributed equally to the study.

The Declaration of Conflict of Interest/ Common Interest
No conflict of interest or common interest has been declared by the authors.

The Declaration of Ethics Committee Approval
This study does not require ethics committee permission or any special permission.

The Declaration of Research and Publication Ethics
The authors of the paper declare that they comply with the scientific, ethical and quotation rules of SAUJS in all processes of the paper and that they do not make any falsification on the data collected. In addition, they declare that Sakarya University Journal of Science and its editorial board have no responsibility for any ethical violations that may be encountered, and that this study has not been evaluated in any academic publication environment other than Sakarya University Journal of Science.

REFERENCES

[1] P. Noblia, M. Vieites, B. S. Parajon-Costa, E. J. Baran, H. Cerecetto, P. Draper, M. Gonzalez, O. E. Piro, E. E. Castellano, A. Azqueta, A. L. de Cerain A. Monge-Vega, D. Gambino, "Vanadium(V) complexes with salicylaldehyde semicarbazone derivatives bearing in vitro anti-tumor activity toward kidney tumor cells (TK-10): crystal structure of [(VO2)-O-V(5-bromosalicylaldehyde semicarbazone)]," Journal of Inorganic Biochemistry, vol. 99, no. 2, pp. 443–451, 2005.

[2] R. K. Mohapatra, A. K. Sarangi, M. Azam, M. M. El-ajaily, M. Kudrat-E-Zahan, S. B. Patjoshi, D. C. Dash, "Synthesis, structural investigations, DFT, molecular docking and antifungal studies of transition metal complexes with benzothiazole based Schiff base ligands," Journal of Molecular Structure, vol. 1179, pp. 65–75, 2019.

[3] T. Vijayan, J. Kim, M. Azam, S. L. Al-Resayes, A. Stalin, B. S. Kannan, M. Jayamani, A. Ayyakannu, S. Nallathambi, "Influence of co-ligand on the biological properties of Schiff base metal complexes: Synthesis, characterization, cytotoxicity, and antimicrobial studies," Applied Organometallic Chemistry, vol. e6542, 2021.

[4] N. Poulter, M. Donaldson, G. Mulley, L. Duque, N. Waterfield, A.G. Shard, S. Spencer, A. T. A. Jenkins, A. L.

Johnson, "Plasma deposited metal Schiff-base compounds as antimicrobials," New Journal of Chemistry, vol. 35, no. 7, pp. 1477–1484, 2011.

[5] M. Azam, S. M. Wabaidur, M. J. Alam, A. Trzesowska-Kruszynska, R. Kruszynski, M. Alam, S. I. Al-Resayes, S. Dwivedi, M. R. Khan, M. S. Islam, N. T. M. Ibaqami, "Synthesis, structural investigations and pharmacological properties of a new zinc complex with a N4-donor Schiff base incorporating 2-pyridyl ring," Inorganica Chimica Acta, vol. 487, pp. 97–106, 2019.

[6] P. G. Cozzi, "Metal-Salen Schiff base complexes in catalysis: practical aspects," Chemical Society Reviews, vol. 33, no. 7, pp. 410–421, 2004.

[7] P. R. Reddy, A. Shilpa, N. Raju, P. Raghavaiah, "Synthesis, structure, DNA binding and cleavage properties of ternary amino acid Schiff base-phen/bipy Cu(II) complexes," Journal of Inorganic Biochemistry, vol. 105, no. 12, pp. 1603–1612, 2011.

[8] D. W. Roberts, T. W. Schultz, A. M. Api, "Skin Sensitization QMM for HRIPT NOEL data: Aldehyde Schiff-Base domain," Chemical Research in Toxicology, vol. 30, no. 6, pp. 1309–1316, 2017.

[9] K. M. Abuamer, A. A. Maihub, M. M. El-Ajaily, A. M. Etorki, M. M. Abou-Krisha, "The role of aromatic Schiff bases in the dyes techniques," International Journal of Organic Chemistry, vol. 04, no. 01, pp. 7–15, 2014.

[10] V. G. Vlasenko, A. S. Burlov, T. A. Kuz'menko, A. T. Kozakov, A. V. Nikol'skii, A. L. Trigub, S. I. Levchenkov, "Synthesis, structure, and X-ray photoelectron spectra of cobalt and copper complexes with 2-{(E)-[2-(4-hydroxybutylami-no)benzimidazol-1-yl]iminomethyl}phenol," Russian Journal of General Chemistry, vol. 88, no. 12, pp. 2550–2558, 2018.

[11] A. K. Satapathy, S. K. Behera, A. Yadav, L. N. Mahour, C. V. Yelamaggad, K. L. Sandhya, B. Sahoo, "Tuning the fluorescence behavior of liquid crystal molecules containing Schiff-base: Effect of solvent polarity," Journal of Luminescence, vol. 210, pp. 371–375, 2019.

[12] B. Mohan, A. Jana, N. Das, S. Bharti, M. Choudhary, S. Muhammad, S. Kumar, A. G. Al-Sehemi, H. Algarni, "A dual approach to study the key features of nickel (II) and copper (II) coordination complexes: Synthesis, crystal structure, optical and nonlinear properties," Inorganica Chimica Acta, vol. 484, pp. 148–159, 2019.

[13] E. W. Schmidt, "Hydrazine and Its Derivatives: Preparation, Properties, Applications," John Wiley & Sons, 2nd ed., 2001.

[14] M. Yuan, D. B. Mitzi, "Solvent properties of hydrazine in the preparation of metal chalcogenide bulk materials and films," Dalton Transactions, pp. 6078–6088, 2009.

[15] S. Basak, K. S. Rane, P. Biswas, "Hydrazine-assisted, low-temperature aerosol pyrolysis method to synthesize γ-Fe2O3," Chemistry Materials, vol. 20, no. 15, pp. 4906–4914, 2008.

[16] R. Dennington II, T. Keith, J. Millam, Gauss View, Version 4.1.2, Semichem Inc, Shawnee Mission, KS, 2007.

[17] M. J. Frisch, G. W. Trucks, H. B. Schlegel, G. E. Scuseria, M. A. Robb, J. R. Cheeseman Jr, J. A. Montgomery, T. Vreven, K. N. Kudin, J. C. Burant, J. M.

Millam, S. S. Iyen-gar, J. Tomasi, V. Barone, B. Mennucci, M. Cossi, G. Scalmani, N. Rega, G. A. Pe-tersson, H. Nakatsuji, M. Hada, M. Ehara, K. Toyota, R. Fukuda, J. Hasegawa, M. Ishida, T. Nakajima, Y. Honda, O. Kitao, H. Nakai, M. Klene, X. Li, J. E. Knox, H. P. Hratchian, J. B. Cross, V. Bakken, C. Adamo, J. Jaramillo, R. Gomperts, R. E. Stratmann, O. Yazyev, R. C. Austin, C. Pomelli, J. W. Ochterski, P. Y. Ay-ala, K. Morokuma, G. A. Voth, P. Salvador, J. J. Dannenberg, V. G. Zakrzewski, S. Dapprich, A. D. Daniels, M. C. Strain, O. Farkas, D. K. Malick, A. D. Rabuck, K. Raghavachari, J. B. Foresman, J. V. Ortiz, Q. Cui, A. G. Baboul, S. Cliford, J. Cioslowski, B. B. Stefanov, G. Liu, A. Liashenko, Piskorz P, I. Komaromi, R. L. Martin, D. J. Fox, T. Keith, M. A. Al-Laham, C. Y. Peng, A. Nanayakkara, M. Challacombe, P. M. W. Gill, B. Johnson, W. Chen, M. W. Wong, C. Gonzalez, J. A. Pople, Gaussian 03, Revision E.01, Gaussian, Inc., Wallingford, CT, 2004.

[18] C. Lee, W. Yang, R. G. Parr, "Development of the Colle-Salvetti correlation-energy formula into a functional of the electron density," Physical Review B, vol. 37, pp. 785–789, 1988.

[19] M. J. Turner, J. J. MacKinnon, S. K. Wolff, D. J. Grimwood, P. R. Spackman, D. Jayatilaka, M. A. Spackman. Crystal explorer Ver. 17.5. University of Western Australia, 2017. http://hirshfeldsurface.net.

[20] Stoe & Cie *X-AREA* and *X-RED32* , Stoe & Cie, Darmstadt, Germany, 2002.

[21] G. M. Sheldrick, "SHELXT - Integrated space-group and crystal-structure determination," Acta Crystallographica Section A: Foundations and Advances, vol. 71, pp. 3–8, 2015.

[22] G. M. Sheldrick, "Crystal Structure Refinement with SHELXL," Acta Crystallographica Section C: Structural Chemistry, vol. 71, pp. 3–8, 2015.

[23] P. R. Spackman, M. J. Turner, J. J. McKinnon, S. K. Wolff, D. J. Grimwood, D. Jayatilaka, M. A. Spackman, "CrystalExplorer: A program for Hirshfeld surface analysis, visualization and quantitative analysis of molecular crystals," Journal of Applied Crystallography, vol. 54, no. 3, pp. 1006-1011, 2021.

[24] M. A. Spackman, D. Jayatilaka, "Hirshfeld surface analysis," Crystal Engineering Communication, vol. 11, pp. 19–32, 2009.

[25] O. Simsek, M. Dincer, N. Dege, E. Saif, I. Yilmaz, A. Cukurovali, "Crystal structure and Hirshfeld surface analysis of (Z)-4-{[4-(3-methyl-3-phenylcyclobutyl) thiazol-2-yl] amino}-4-oxobut-2-enoic acid," Acta Crystallographica Section E: Crystallographic Communications, vol. 78, no. 2, pp. 120–124, 2022.

[26] R. Yankova, I. Tankov, T. Tsaneva, "Crystal structure, intermolecular interactions and NLO properties for imidazolium hydrogen sulfate ionic liquid," Journal of Molecular Structure, vol. 1273, pp. 134307, 2023.

[27] S. Atalay, M. Macit, H. Bulbul, "Crystal structure and computational studies of N-((2-ethoxynaphthalen-1-yl) methylene)-4-fluoroaniline," European Journal of Chemistry, vol. 12, no. 4, pp. 454-458, 2021.

[28] M. N. Tahir, A. Ali, M. Khalid, M. Ashfaq, M. Naveed, S. Murtaza, I. Shafiq, M. A. Asghar, R. Orfali, S. Perveen, "Efficient synthesis of imine-carboxylic acid functionalized compounds: Single crystal, Hirshfeld

surface and quantum chemical exploration," Molecules, vol. 28, no. 7, pp. 2967, 2023.

[29] H. Gökce, F. Şen, Y. Sert, B. F. Abdel-Wahab, B. M. Kariuki, G. A. El-Hiti, "Quantum computational investigation of (E)-1-(4-methoxyphenyl)-5-methyl-N′-(3-phenoxybenzylidene)-1 H-1, 2, 3-triazole-4-carbohydrazide," Molecules, vol. 27, no. 7, pp. 2193, 2022.

[30] G. Kaştaş, Ç. A. Kaştaş, "Scrutinizing the two new o-hydroxy Schiff bases from the point of tautomeric behavior and non-covalent interactions (H-bond, Br··· Br, π··· π and CH··· π) in their supramolecular architectures," Journal of Molecular Structure, vol. 1184, pp. 427-434, 2019.

[31] M. R. Albayati, S. Kansız, H. Lgaz, S. Kaya, N. Dege, I. H. Ali, R. Salghi, I. M. Chung, "Synthesis, experimental and theoretical characterization of (E)-2-((2, 3-dimethylphenyl) amino)-N'-(furan-2-ylmethylene) benzohydrazide," Journal of Molecular Structure, vol. 1219, pp. 128518, 2020.

[32] A. A. B. OmarAli, A. J. M. Al-Karawi, N. Dege, S. Kansız, H. A. Ithawi, "Synthesis and X-ray crystal structures of two different zinc (II) complexes of N, N′-cyclohexane-1, 2-diylidene-bis (4-fluorobenzoylhydrazide) based on zinc salt effect," Journal of Molecular Structure, vol. 1217, pp. 128387, 2020.

[33] A. A. OmarAli, A. J. M. Al-Karawi, A. A. Awad, N. Dege, S. Kansız, E. Agar, Z. A. Hussein, I. R. Mohammed, "Two new zinc (II) and mercury (II) complexes based on N, N′-(cyclohexane-1, 2-diylidene) bis (4-fluorobenzohydrazide): synthesis, crystal structures and antibacterial activities," Acta Crystallographica Section C: Structural Chemistry, vol. 76, no. 5, pp. 476-482, 2020.

[34] R. Sathyanarayanan, M. Selvapandiyan, C. Senthilkumar, M. Srinivasan, P. Ramasamy, "Crystal growth, Hirshfeld surface, quantum chemical calculations, optical, photoluminescence and thermal analyses of sodium D-isoascorbate monohydrate single crystal," Journal of Molecular Structure, vol. 1275, pp. 134637, 2023.

[35] A. Gannouni, W. Tahri, T. Roisnel, S. I. Al-Resayes, M. Azam, R. Kefi, "Single crystal investigations, Hirshfeld surface analysis, DFT studies, molecular docking, physico-chemical characterization, and biological activity of a novel non-centrosymmetric compound with a copper transition metal precursor," ACS Omega, vol. 8, no. 8, pp. 7738-7748, 2023.

[36] J. Makhlouf, Y. El Bakri, A. Valkonen, K. Saravanan, S. Ahmad, W. Smirani, "Growth, single crystal investigations, hirshfeld surface analysis, DFT studies, molecular dynamics simulations, molecular docking, physico-chemical characterization and biological activity of novel thiocyanic complex with zinc transition metal precursor," Polyhedron, vol. 222, pp. 115937, 2022.

[37] R. Saddik, S. A. Brandán, S. Mortada, C. Baydere, O. Roby, N. Dege, S. Tighadouini, M. Tahiri, M. A. Faouzi, K. Karrouchi, "Synthesis, crystal structure, Hirshfeld surface analysis, DFT and antihyperglycemic activity of 9-allyl-2, 3, 9, 10a-tetrahydrobenzo [b] cyclopenta [e][1, 4] diazepin-10 (1H)-one," Journal of Molecular Structure, vol. 1283, pp. 135283, 2023.

[38] L. Guo, B. Tan, X. Zuo, W. Li, S. Leng, X. Zheng, "Eco-friendly food spice 2-Fur-furylthio-3-methylpyrazine as an

excellent inhibitor for copper corrosion in sulfuric acid medium," Journal of Molecular Liquids, vol. 317, 113915, 2020.

[39] Z. Demircioğlu, G. Kaştaş, Ç.A. Kaştaş, R. Frank, "Spectroscopic, XRD, Hirshfeld surface and DFT approach (chemical activity, ECT, NBO, FFA, NLO, MEP, NPA&MPA) of (E)-4-bromo-2-[(4- bromophenylimino) methyl]-6-ethoxyphenol," Journal of Molecular Structure, vol. 1191, pp. 129–137, 2019.

[40] H. Lgaz, R. Salghi, S. Masroor, S.H. Kim, C. Kwon, S.Y. Kim, Y.J. Yang, I.M. Chung, "Assessing corrosion inhibition characteristics of hydrazone derivatives on mild steel in HCl: insights from electronic-scale DFT and atomic-scale molecular dynamics," Journal of Molecular Liquids, vol. 308, 112998, 2020.

[41] M. Azam, P.K. Sahoo, R.K. Mohapatra, M. Kumar, A. Ansari, I.S. Moon, A. Chutia, S.I. Resays, S.K. Biswal, "Structural investigations, Hirsfeld surface analyses, and molecular docking studies of a phenoxo-bridged binuclear zinc(II) complex," Journal of Molecular Structure, vol. 1251, 132039, 2022.

[42] S. I. Al-Resayes, M. Azam, A. Trzesowska-Kruszynska, R. Kruszynski, S. M. Soliman, R. K. Mohapatra, Z. Khan, "Structural and theoretical investigations, Hirshfeld surface analyses, and cytotoxicity of a naphthalene-based chiral compound," ACS Omega, vol. 5, pp. 27227–27234, 2020.

[43] A. Saeed, S. Ashraf, U. Flörke, Z. Y. D. Espinoza, M. F. Erben, H. Pérez, "Supramolecular self-assembly of a coumarine-based acylthiourea synthon directed by π-stacking interactions: Crystal structure and Hirshfeld surface analysis," Journal of Molecular Structure, vol. 1111, pp. 76-83, 2016.

[44] S. Adhikari, A. H. Sheikh, S. Kansız, N. Dege, N. Baildya, G. Mahmoudi, N. A. Choudhury, R. J. Butcher, W. Kaminsky, S. Talledo, E. M. Lopato, S. Bernhard, J. Kłak, "Supramolecular Co (II) complexes based on dithiolate and dicarboxylate ligands: Crystal structures, theoretical studies, magnetic properties, and catalytic activity studies in photocatalytic hydrogen evolution," Journal of Molecular Structure, pp. 135481, 2023.

[45] M. K. Gümüş, S. Kansiz, G. B. Tulemisova, N. Dege, E. Saif, "Crystal structure and Hirshfeld surface analysis of 3-(hydroxymethyl)-3-methyl-2, 6-diphenylpiperidin-4-one," Acta Crystallographica Section E: Crystallographic Communications, vol. 78, no. 1, pp. 29-32, 2022.

[46] D. M. Al-thamili, A. I. Almansour, N. Arumugam, S. Kansız, N. Dege, S. M. Soliman, M. Azam, R. S. Kumar, "Highly functionalized N-1-(2-pyridinylmethyl)-3, 5-bis [(E)-arylmethylidene] tetrahydro-4 (1H)-pyridinones: Synthesis, characterization, crystal structure and DFT studies," Journal of Molecular Structure, vol. 1222, pp. 128940, 2020.

[47] Z. Setifi, N. Cubillán, C. Glidewell, D. M. Gil, E. Torabi, M. Morales-Toyo, N. Dege, F. Setifi, M. Mirzaei, "A combined experimental, Hirshfeld surface analysis, and theoretical study on fac-[tri (azido)(tris (2-pyridyl) amine) iron (III)]," Polyhedron, vol. 233, pp. 116320, 2023.